Mechanics Research Communications 112 (2021) 103599

Contents lists available at ScienceDirect

Mechanics Research Communications

journal homepage: www.elsevier.com/locate/mechrescom

A posteriori error estimates in a finite element VMS-based reduced order model for the incompressible Navier-Stokes equations

Ramon Codina*, Ricardo Reyes, Joan Baiges

Department of Civil and Environmental Engineering, Technical University of Catalonia Jordi Girona 1-3, Edifici C1., Barcelona 08034, Spain

ARTICLE INFO

Article history:
Received 28 April 2020
Revised 18 September 2020
Accepted 20 September 2020
Available online 16 October 2020

Keywords:
A posteriori error estimates
Reduced order model
Variational multi-scale method
Incompressible flows

ABSTRACT

In this paper we present an a posteriori error estimate for a reduced order model (ROM) for the incompressible Navier-Stokes equations that is based on the fact that the full order model is a finite element (FE) approximation. Both this FE approximation and the ROM are stabilized by means of a variational multi-scale (VMS) strategy, in which the unknowns are split into FE scales and sub-grid scales (SGS), the latter being modeled in terms of the former. The SGS, when properly scaled, provide directly the a posteriori error estimate, both for the ROM and for the FE approximation.

1. Introduction

In this paper we consider a reduced order model (ROM) for the incompressible Navier-Stokes equations that assumes that the full order model (FOM) is a finite element (FE) method based on the Variational Multi-scale (VMS) concept [14,28]; this ROM has been proposed in [43]. The idea is to construct a ROM basis using a proper orthogonal decomposition (POD) from a collection of FOM snapshots (i.e., solutions at certain time steps) and then apply exactly the same VMS formulation as in the FOM, but using the ROM basis instead of the standard FE basis (see for example [20,21,49] for a description of POD).

The need to use some sort of stabilized formulation for the ROM is the same as for the FOM. In the case of the incompressible Navier-Stokes equations approximated using the FE method, this need arises essentially from the compatibility of the velocity and pressure interpolations and from the possibility of having to deal with convection-dominated flows. This is why different ROM formulations have been proposed introducing some sort of stabilization, such as SUPG-type methods [8,22,38], a VMS approach different to the one we propose here [8], term by term stabilizations [2,29,30,33,44], and some empirical methods [1,6,32,51]. A standard residual-based VMS method followed either by a projection onto the ROM space or by a projection of the Galerkin equations is proposed in [46], the latter case requiring a specific pressure stabilization through what is called pressure supremizer in the paper.

The numerical analysis of VMS-type FE formulations is already mature, at least for linear and stationary problems. Conditions under which stability and a priori error estimates can be obtained are well understood. Once the FE approximation has been obtained, standard techniques to obtain a posteriori error estimates can be used, although it is also possible to make use of the ideas underlying the VMS concept, as done in [25,26] and already sketched in [28]; in fact, it would even be possible to solve for the SGS in a mesh finer than the FE scales, and use this as a posteriori error estimation [34,35,37]. This is precisely what we favor: since the continuous solution is split into the FE component and a sub-grid scale (SGS), the better the approximation to this SGS, the closer it will be to the true error, i.e., the SGS can be used for the a posteriori error estimation. However, this idea needs to be elaborated, and answer questions such as the norm in which this a posteriori error has to be understood, or what is the adequate scaling to include velocities and pressures in a single estimate. We have discussed previously this idea in [3].

The seemingly straightforward idea that we propose here has limitations. The a posteriori error estimate provides the error in each element of the FE partition and, since it replaces an a priori error estimate which bounds the error in terms of the mesh size, h, it also gives information about the behavior of the error in terms of h. However, in the ROM one has no access to modifying h, which has been used to obtain the FOM solution. What would be needed is an a posteriori error estimate that would express the error in terms of ROM parameters, and in particular in terms of the components disregarded in the POD decomposition. A priori estimates in this sense rely on the very general Eckart-Young-Mirsky theorem, independent of the problem being solved, and in which the

* Corresponding author.
E-mail address: ramon.codina@upc.edu (R. Codina).

https://doi.org/10.1016/j.mechrescom.2020.103599
0093-6413/

error depends solely on the number of singular values kept in the approximation over the total number of singular values that would expand the FOM space.

This discussion explains why adaptivity in ROM has been implemented mainly in the construction of the basis functions from the FOM solutions, as in [16,23,48]; h-adaptivity in the calculation of the basis is formulated in [10,19]. Adaptivity in the selection of the basis functions is proposed in [40,41,47]. In all these references, adaptivity is not directly based on an a posteriori error estimation for the ROM, as the one we propose in this paper. This is also done in [36] with an a posteriori estimate based on the residuals for the Stokes and Darcy systems coupled through an interface.

Although we will not exploit it here, the a posteriori error estimate we propose in this paper can be used in the hyper-reduction strategy proposed in [42], in which the advective term of the Navier-Stokes equations is computed in a mesh coarser than the one used in the FOM. This strategy is similar to the one proposed in [50] (see also [24]), and has to be considered as an alternative to the sampling-based algorithms for hyper-reduction [4,7,11,27,39,45]. In [42] the a posteriori error estimate was simply set, not elaborated. Here we justify it, compute its effectivity index in a numerical example and discuss its performance.

This paper is organized as follows. In the next section we present the VMS-ROM formulation we propose for the incompressible Navier-Stokes equations, following the one proposed in [43]. In Section 3 we state the proposed a posteriori error estimate, based on the SGS. In Section 4 we provide some theoretical foundation for it and in Section 5 we present two numerical examples to show its behavior. Conclusions close the paper in Section 6.

2. VMS-ROM for the incompressible Navier-Stokes equations

2.1. Incompressible Navier-Stokes equations

Let Ω be a bounded domain of $\mathbb{R}^d$ $(d = 2, 3)$ where the fluid flows during the time interval $]0, t_f[$. Let $\boldsymbol{u} : \Omega \times]0, t_f[\to \mathbb{R}^d$ be the velocity field, $p : \Omega \times]0, t_f[\to \mathbb{R}$ the pressure and $\boldsymbol{f} : \Omega \times]0, t_f[\to \mathbb{R}^d$ the field of body forces. For a given $\boldsymbol{a} : \Omega \times]0, t_f[\to \mathbb{R}^d$, assumed to be divergence free, we define the operator $\mathcal{L}_1$ of d components, the operator $\mathcal{L}_2$ of one component, and the combination $\mathcal{L} = [\mathcal{L}_1, \mathcal{L}_2]$, as

$$\begin{aligned}\mathcal{L}(\boldsymbol{a}; [\boldsymbol{u}, p]) &:= [\mathcal{L}_1(\boldsymbol{a}; [\boldsymbol{u}, p]), \mathcal{L}_2(\boldsymbol{u})] \\ &:= [-\nu\Delta\boldsymbol{u} + \boldsymbol{a}\cdot\nabla\boldsymbol{u} + \nabla p, \nabla\cdot\boldsymbol{u}],\end{aligned}$$

where ν is the kinematic viscosity of the fluid. We also define the operator of $d \times d$ components

$$\mathcal{F}([\boldsymbol{u}, p]) = \nu\nabla\boldsymbol{u} - p\boldsymbol{I}_d,$$

where $\boldsymbol{I}_d$ is the identity matrix in $\mathbb{R}^d$.

Let us consider the boundary $\partial\Omega$ split into two disjoint sets Γ_D and Γ_N, on which we shall prescribe homogenous (for simplicity) Dirichlet and Neumann conditions, respectively. If $\boldsymbol{u}^0$ is the initial velocity field, the incompressible Navier-Stokes problem consists in finding a velocity $\boldsymbol{u}$ and a pressure p such that

$$\begin{aligned}[\partial_t\boldsymbol{u}, 0] + \mathcal{L}(\boldsymbol{u}; [\boldsymbol{u}, p]) &= [\boldsymbol{f}, 0] && \text{in } \Omega,\ t \in]0, t_f[, \\ \boldsymbol{u} &= \boldsymbol{0} && \text{on } \Gamma_D,\ t \in]0, t_f[, \\ \boldsymbol{n}\cdot\mathcal{F}([\boldsymbol{u}, p]) &= \boldsymbol{0} && \text{on } \Gamma_N,\ t \in]0, t_f[, \\ \boldsymbol{u} &= \boldsymbol{u}^0 && \text{in } \Omega,\ t = 0,\end{aligned}$$

where $\boldsymbol{n}$ is the unit normal exterior to the boundary of the domain where it is evaluated, in this case the boundary Γ_N of Ω.

To write the weak form of the problem, let $\langle\,\cdot\,,\,\cdot\,\rangle_\omega$ be the integral of the product of two functions in a domain ω, the subscript being omitted when $\omega = \Omega$. Let us also introduce

$$\begin{aligned}B_\omega(\boldsymbol{a}; [\boldsymbol{u}, p], [\boldsymbol{v}, q]) &:= \nu\langle\nabla\boldsymbol{u}, \nabla\boldsymbol{v}\rangle_\omega \\ &+ \langle\boldsymbol{a}\cdot\nabla\boldsymbol{u}, \boldsymbol{v}\rangle_\omega - \langle p, \nabla\cdot\boldsymbol{v}\rangle_\omega + \langle q, \nabla\cdot\boldsymbol{u}\rangle_\omega, \qquad (1)\end{aligned}$$

$$L_\omega([\boldsymbol{v}, q]) := \langle\boldsymbol{f}, \boldsymbol{v}\rangle_\omega. \qquad (2)$$

To have well defined forms B_ω and L_ω for all $t \in]0, t_f[$, let V the space of functions where $\boldsymbol{a}(\,\cdot\,, t)$, $\boldsymbol{u}(\,\cdot\,, t)$ and $\boldsymbol{v}$ should belong, and Q the space of $p(\,\cdot\,, t)$ and q; V is a subspace of $H^1(\Omega)^d$ and $Q = L^2(\Omega)$. The weak form of the problem (in space) consists of finding $\boldsymbol{u}$: $]0, t_f[\to V$ and p: $]0, t_f[\to Q$ such that

$$\begin{aligned}\langle\partial_t\boldsymbol{u}, \boldsymbol{v}\rangle + B_\Omega(\boldsymbol{u}; [\boldsymbol{u}, p], [\boldsymbol{v}, q]) &= L_\Omega([\boldsymbol{v}, q]), \qquad (3) \\ \langle\boldsymbol{u}, \boldsymbol{v}\rangle &= \langle\boldsymbol{u}^0, \boldsymbol{v}\rangle, \quad \text{at } t = 0\end{aligned}$$

for all $\boldsymbol{v} \in V$ and $q \in Q$.

2.2. VMS-FOM approximation

Let $\mathcal{P}_h = \{K\}$ a FE partition of the domain Ω, assumed for simplicity quasi-uniform with elements of size h. From this we may construct conforming FE spaces $V_h \subset V$ and $Q_h \subset Q$ in the usual manner.

Let us define the formal adjoints of the operators $\mathcal{L}$ and $\mathcal{F}$ as

$$\begin{aligned}\mathcal{L}^*(\boldsymbol{a}; [\boldsymbol{v}, q]) &:= [-\nu\Delta\boldsymbol{v} - \boldsymbol{a}\cdot\nabla\boldsymbol{v} - \nabla q, -\nabla\cdot\boldsymbol{v}], \\ \mathcal{F}^*(\boldsymbol{a}; [\boldsymbol{v}, q]) &:= \nu\nabla\boldsymbol{v} + q\boldsymbol{I}_d + \boldsymbol{a}\otimes\boldsymbol{v}.\end{aligned}$$

It is readily checked that these operators allow us to write, for smooth enough functions:

$$\begin{aligned}&B_\Omega(\boldsymbol{a}; [\boldsymbol{u}, p], [\boldsymbol{v}, q]) \\ &= \sum_K B_K(\boldsymbol{a}; [\boldsymbol{u}, p], [\boldsymbol{v}, q]) \\ &= \sum_K \langle\mathcal{L}(\boldsymbol{a}; [\boldsymbol{u}, p]), [\boldsymbol{v}, q]\rangle_K + \sum_K \langle\boldsymbol{n}\cdot\mathcal{F}([\boldsymbol{u}, p]), \boldsymbol{v}\rangle_{\partial K} \\ &= \sum_K \langle[\boldsymbol{u}, p], \mathcal{L}^*(\boldsymbol{a}; [\boldsymbol{v}, q])\rangle_K + \sum_K \langle\boldsymbol{u}, \boldsymbol{n}\cdot\mathcal{F}^*(\boldsymbol{a}; [\boldsymbol{v}, q])\rangle_{\partial K}. \qquad (4)\end{aligned}$$

Let $\mathcal{E}_h = \{E\}$ be the collection of edges (faces, if $d = 3$) of $\mathcal{P}_h$. Note that, if $\boldsymbol{v}$ is continuous across elements,

$$\sum_K \langle\boldsymbol{n}\cdot\mathcal{F}([\boldsymbol{u}, p]), \boldsymbol{v}\rangle_{\partial K} = \sum_E \langle[\![\boldsymbol{n}\cdot\mathcal{F}([\boldsymbol{u}, p])]\!], \boldsymbol{v}\rangle_E, \qquad (5)$$

where the jump of the flux is defined as

$$[\![\boldsymbol{n}\cdot\mathcal{F}([\boldsymbol{u}, p])]\!] = \boldsymbol{n}\cdot\mathcal{F}([\boldsymbol{u}, p])|_{\partial K_1} + \boldsymbol{n}\cdot\mathcal{F}([\boldsymbol{u}, p])|_{\partial K_2},$$

being K_1 and K_2 the elements that share edge E. In Eq. (5) it is understood that for the edges belonging to Γ_N only the interior element contributes to the jump (recall that the Neumann boundary condition is taken as homogeneous). A similar remark is applicable to the last term in Eq. (4).

The key idea of the VMS approach is to consider the splitting $V = V_h \oplus V'$, $Q = Q_h \oplus Q'$, where V' and Q' are any spaces that complete V_h in V and Q_h in Q, respectively. These will be called the spaces of sub-grid scales (SGS). Functions in the FE spaces will be identified with the subscript h, whereas functions in the SGS spaces will be identified with the superscript $'$. From the splitting $\boldsymbol{u} = \boldsymbol{u}_h + \boldsymbol{u}'$, $p = p_h + p'$ and similarly for the test functions $\boldsymbol{v} = \boldsymbol{v}_h + \boldsymbol{v}'$, $q = q_h + q'$, and using Eq. (4), it turns out that Eq. (3) is equivalent to

$$\begin{aligned}&\langle\partial_t\boldsymbol{u}_h + \partial_t\boldsymbol{u}', \boldsymbol{v}_h\rangle + B_\Omega(\boldsymbol{u}; [\boldsymbol{u}_h, p_h], [\boldsymbol{v}_h, q_h]) \\ &+ \sum_K \langle[\boldsymbol{u}', p'], \mathcal{L}^*(\boldsymbol{u}; [\boldsymbol{v}_h, q_h])\rangle_K \\ &+ \sum_E \langle\boldsymbol{u}', [\![\boldsymbol{n}\cdot\mathcal{F}^*(\boldsymbol{u}; [\boldsymbol{v}_h, q_h])]\!]\rangle_E \\ &= L([\boldsymbol{v}_h, q_h]) \quad \forall [\boldsymbol{v}_h, q_h] \in V_h \times Q_h, \qquad (6)\end{aligned}$$

$$\langle \partial_t \boldsymbol{u}_h + \partial_t \boldsymbol{u}', \boldsymbol{v}' \rangle + \sum_K \langle \mathcal{L}(\boldsymbol{u}; [\boldsymbol{u}_h, p_h]) + \mathcal{L}(\boldsymbol{u}; [\boldsymbol{u}', p']), [\boldsymbol{v}', q'] \rangle_K + \sum_K \langle \boldsymbol{n} \cdot \mathcal{F}([\boldsymbol{u}_h, p_h]) + \boldsymbol{n} \cdot \mathcal{F}([\boldsymbol{u}', p']), \boldsymbol{v}' \rangle_{\partial K} = L([\boldsymbol{v}', q']) \quad \forall [\boldsymbol{v}', q'] \in V' \times Q'. \tag{7}$$

These equations, to which initial conditions have to be appended, are exactly equivalent to the continuous problem. It is at this point where approximations and possible choices need to be made. In our case, these are (see [14] for details):

- V' is taken as L^2 orthogonal to V_h, yielding the Orthogonal SGS (OSGS) formulation.
- The transport velocity $\boldsymbol{u} = \boldsymbol{u}_h + \boldsymbol{u}'$ is approximated by $\boldsymbol{u}_h$ (this can be relaxed, see [12]).
- (Key approximation) The operator $\mathcal{L}$ is approximated as [12]:

$$\mathcal{L}(\boldsymbol{a}; [\boldsymbol{u}', p']) \approx [\tau_{1,K}^{-1} \boldsymbol{u}', \tau_{2,K}^{-1} p'],$$

$$\tau_{1,K}^{-1} = c_1 \frac{\nu}{h^2} + c_2 \frac{|\boldsymbol{a}|}{h}, \tag{8}$$

$$\tau_{2,K} = \nu + \frac{c_2}{c_1} |\boldsymbol{a}| h, \tag{9}$$

  where c_1 and c_2 are algorithmic constants.
- (Key approximation) On each $E \in \mathcal{E}_h$, $\boldsymbol{u}'$ is approximated by [15]:

$$\boldsymbol{u}'|_E \approx -\tau_E [\![\boldsymbol{n} \cdot \mathcal{F}([\boldsymbol{u}_h, p_h])]\!], \tag{10}$$

$$\tau_E = c_3 \frac{h}{\nu}, \tag{11}$$

  where c_3 is another algorithmic constant.
- Approximation (10) being motivated by the fact that the total flux has to be continuous, it is assumed that

$$\sum_K \langle \boldsymbol{n} \cdot \mathcal{F}([\boldsymbol{u}_h, p_h]) + \boldsymbol{n} \cdot \mathcal{F}([\boldsymbol{u}', p']), \boldsymbol{v}' \rangle_{\partial K} = 0$$

  for all $\boldsymbol{v}' \in V'$.

From all these items, the final discrete approximation to (6) and (7) is

$$\langle \partial_t \boldsymbol{u}_h, \boldsymbol{v}_h \rangle + B_\Omega(\boldsymbol{u}_h; [\boldsymbol{u}_h, p_h], [\boldsymbol{v}_h, q_h]) + \sum_K \langle \boldsymbol{u}'_K, \mathcal{L}_1^*(\boldsymbol{u}_h; [\boldsymbol{v}_h, q_h]) \rangle_K - \sum_K \langle p'_K, \nabla \cdot \boldsymbol{v}_h \rangle_K - \sum_E \langle \boldsymbol{u}'_E, [\![\boldsymbol{n} \cdot \mathcal{F}^*(\boldsymbol{u}_h; [\boldsymbol{v}_h, q_h])]\!] \rangle_E = L([\boldsymbol{v}_h, q_h]) \quad \forall [\boldsymbol{v}_h, q_h] \in V_h \times Q_h, \tag{12}$$

$$\partial_t \boldsymbol{u}'_K + \tau_{1,K}^{-1} \boldsymbol{u}'_K = P^\perp(\boldsymbol{f} - \mathcal{L}_1(\boldsymbol{u}_h; [\boldsymbol{u}_h, p_h])), \tag{13}$$

$$\tau_{2,K}^{-1} p'_K = -P^\perp(\nabla \cdot \boldsymbol{u}_h), \tag{14}$$

$$\tau_E^{-1} \boldsymbol{u}'_E = -[\![\boldsymbol{n} \cdot \mathcal{F}([\boldsymbol{u}_h, p_h])]\!], \tag{15}$$

where $P^\perp$ is the projection L^2 orthogonal to the appropriate FE space, either V_h or Q_h. Note that while p'_K and $\boldsymbol{u}'_E$ can be directly inserted into Eq. (12) Eq. (13) needs to be integrated in time, and therefore values of $\boldsymbol{u}'_K$ at previous time steps of the time discretization need to be stored. Let us also note that in our implementation we evaluate the orthogonal projection iteratively, i.e., for any function f we approximate $P^\perp(f^i) = f^i - P(f^{i-1})$, where the superscript is the iteration counter and P is the L^2 projection onto the FE space. Let us also remark that we may evaluate the last term in the left-hand-side of Eq. (12) as explained in [3], where use is made of the approximation described in [9,17]. In particular, we do this approximation when evaluating the a posteriori error estimator in Section 3.

Any time integration scheme can be used. For conciseness, we shall assume that a backward difference (BDF) scheme is employed. The time interval is assumed to be discretized using a uniform partition of size δt. The time derivative ∂_t has to be replaced by a difference increment of the desired order δ_t, involving the unknowns at the current time step as well as at previous time steps. Using a superscript for the time step counter, the objective is to find the sets $\{\boldsymbol{u}_h^n\} \subset V_h$, $\{p_h^n\} \subset Q_h$, n running from 1 to the number of time steps and $\boldsymbol{u}_h^0$ being determined by the initial condition. For the SGS scale, we may take $\boldsymbol{u}_K'^0 = \boldsymbol{0}$.

2.3. VMS-ROM approximation

We consider the FE approximation described above as a FOM for which we wish to design a ROM. Let $X = V \times Q$ be the space of the continuous problem and $X_h = V_h \times Q_h$ the FE space, with $X' = V' \times Q'$ the space of SGS. Now we wish to construct a ROM space $X_r \subset X_h \subset X$. To this end, we use the classical POD strategy. Suppose that $\{[\boldsymbol{u}_h^{n_1}, p_h^{n_1}], [\boldsymbol{u}_h^{n_2}, p_h^{n_2}], \ldots, [\boldsymbol{u}_h^{n_S}, p_h^{n_S}]\}$ is a collection of snapshots, i.e., solutions of the FOM at time steps $n_1, n_2, \ldots, n_S$. Using the POD we may obtain a ROM space

$$X_r = \text{span}\{\boldsymbol{\varphi}_1, \boldsymbol{\varphi}_2, \ldots, \boldsymbol{\varphi}_r\}.$$

where $r = \dim X_r \ll \dim X_h$. Note that the basis vectors $\boldsymbol{\varphi}_i$, $i = 1, \ldots, r$, contain both velocity and pressure components.

The VMS-ROM formulation we propose is easy to describe: we apply *exactly* the same VMS formulation as for the FOM, just considering functions approximated in X_r instead of X_h. The reason why this is possible relies on the fact that $X_r \subset X_h$ and, in particular, $\boldsymbol{\varphi}_i$, $i = 1, \ldots, r$, can be written as a linear combination of the basis of X_h and therefore these functions will be piecewise polynomials defined on the FE partition $\mathcal{P}_h$. This also justifies why the stabilization parameters can be taken exactly the same.

Applying the VMS concept to the ROM we will have the decompositions

$$X = X_h \oplus X' = X_r \oplus X'',$$

where now X'' is the space of SGS of the ROM space.

Suppose that we were able to construct a POD basis of X_h, with $N = \dim X_h$, i.e.,

$$X_h = \text{span}\{\boldsymbol{\varphi}_1, \boldsymbol{\varphi}_2, \ldots, \boldsymbol{\varphi}_N\}.$$

Then, since the basis vectors obtained from the POD are orthogonal, the choice of orthogonal SGS allows us to write

$$X'' = \text{span}\{\boldsymbol{\varphi}_{r+1}, \boldsymbol{\varphi}_{r+2}, \ldots, \boldsymbol{\varphi}_N\} \oplus X', \tag{16}$$

i.e., we have an explicit representation of the ROM space of SGS. It has to be remarked that the orthogonality of the SGS holds with respect to the mass matrix as inner product, i.e., the Gramm matrix associated to the L^2 inner product of the basis in V_h for the velocity components and of Q_h for the pressure components. This mass matrix has to be given to the POD algorithm to ensure that the basis vectors $\boldsymbol{\varphi}_i$, $i = 1, \ldots, r$, are also orthogonal with respect to it. However, we have found little difference if the orthogonality of the POD basis is imposed with respect to the identity matrix. The difference should be significant in highly non-uniform meshes, but we have not yet explored this point.

In [5] we used a similar approach to the one presented here, the crucial difference being that there we assumed that the best we could hope for the ROM solution was to be close to the FOM one, and thus the ROM SGS should stay in X_h. This led us to consider $X'' = \text{span}\{\boldsymbol{\varphi}_{r+1}, \boldsymbol{\varphi}_{r+2}, \ldots, \boldsymbol{\varphi}_N\}$ instead of (16). Even though the resulting formulation works (after introducing some limits in

the estimation of the parameters), the method described here turns out to be more robust.

Having in mind the previous discussion, the final problem to be solved, already discretized in time, consists in finding $\{[\boldsymbol{u}_r^n, p_r^n]\} \subset V_r \times Q_r$, $n = 1, 2, \ldots$, such that

$$\begin{aligned}&\langle \delta_t \boldsymbol{u}_r, \boldsymbol{v}_r\rangle + B_\Omega(\boldsymbol{u}_r; [\boldsymbol{u}_r, p_r], [\boldsymbol{v}_r, q_r])\\ &\quad + \sum_K \langle \boldsymbol{u}_K'', \mathcal{L}_1^*(\boldsymbol{u}_r; [\boldsymbol{v}_r, q_r])\rangle_K - \sum_K \langle p_K'', \nabla\cdot\boldsymbol{v}_r\rangle_K\\ &\quad - \sum_E \langle \boldsymbol{u}_E'', [\![\boldsymbol{n}\cdot\mathcal{F}^*(\boldsymbol{u}_r; [\boldsymbol{v}_r, q_r])]\!]\rangle_E\\ &\quad = L([\boldsymbol{v}_r, q_r]) \quad \forall [\boldsymbol{v}_r, q_r] \in V_r \times Q_r,\end{aligned} \tag{17}$$

$$\delta_t \boldsymbol{u}_K'' + \tau_{1,K}^{-1}\boldsymbol{u}_K'' = P^\perp(\boldsymbol{f} - \mathcal{L}_1(\boldsymbol{u}_r; [\boldsymbol{u}_r, p_r])), \tag{18}$$

$$\tau_{2,K}^{-1} p_K'' = -P^\perp(\nabla\cdot\boldsymbol{u}_r), \tag{19}$$

$$\tau_E^{-1}\boldsymbol{u}_E'' = -[\![\boldsymbol{n}\cdot\mathcal{F}([\boldsymbol{u}_r, p_r])]\!]. \tag{20}$$

Note that we are making use of the fact that there is an underlying FE partition and that the ROM basis functions are piecewise polynomials defined on it.

It is also important to note, that since the definition of the stabilization parameters only depends on the operators and a characteristic length (Eqs. (8), (9) and (11)) we can use the same parameters for the FOM and ROM cases, as is described in [43].

3. Sub-grid scales as a posteriori error estimates

The following comments apply to both the FE approximation and to the ROM based on it. Let us consider this last situation. The starting point of the VMS approximation is the splitting $\boldsymbol{u} = \boldsymbol{u}_r + \boldsymbol{u}''$ and $p = p_r + p''$. After writing the continuous problem without derivatives on $\boldsymbol{u}''$ and p'', these SGS are then approximated. If this approximation is accurate enough, the SGS directly yield an error estimate, since their approximation, still denoted $[\boldsymbol{u}'', p'']$, should satisfy $[\boldsymbol{u}'', p''] \approx [\boldsymbol{u} - \boldsymbol{u}_r, p - p_r]$. It is hopeless to expect that this estimate will be valid point-wise, but the idea is that it could hold in a certain integral sense.

There are two main questions to address, namely, which is the norm in which $[\boldsymbol{u}'', p'']$ can be considered an a posteriori error estimate and how should velocity and pressure errors be combined in order to obtain an estimate with correct scaling. The answer to both questions is a consequence of which is the norm in which stability and a priori error estimates can be found. As far as we are aware, this analysis for the full transient nonlinear problem is not complete, in the sense that there are no estimates that do not blow up as the viscosity goes to zero (or as the Reynolds number grows). However, such estimates do exist for the stationary linear problem [13], and therefore one may expect that they could be extended to the general case. The spatial norm in which they should hold is

$$\begin{aligned}|||[\boldsymbol{v}, q]|||^2 &= \nu\|\nabla\boldsymbol{v}\|^2 + \sum_K \tau_{1,K}\|\boldsymbol{a}\cdot\nabla\boldsymbol{v} + \nabla q\|_K^2\\ &\quad + \sum_K \tau_{2,K}\|\nabla\cdot\boldsymbol{v}\|_K^2 + \sum_E \tau_E\|[\![\boldsymbol{n}q]\!]\|_E^2,\end{aligned} \tag{21}$$

where $\boldsymbol{a}$ is the advection velocity, $\|\cdot\|$ the L^2 norm over Ω and $\|\cdot\|_\omega$ the L^2 norm over ω, for $\omega = K, E$. For transient problems, the expected norm is the discrete L^2 norm in time of this spatial norm. Note that for continuous pressures the last term vanishes.

Let $\eta_K([\boldsymbol{u}'', p''])$ be the contribution of element K to the a posteriori error estimate. *The design of η_K we propose is*:

$$\eta_K^2([\boldsymbol{u}'', p'']) = \int_K \tau_{1,K}^{-1}|\boldsymbol{u}_K''|^2 + \int_K \tau_{2,K}^{-1}|p_K''|^2 + \frac{1}{2}\sum_{E\subset\partial K}\int_E \tau_E^{-1}|\boldsymbol{u}_E''|^2. \tag{22}$$

This means that we claim that

$$|||[\boldsymbol{u} - \boldsymbol{u}_r, p - p_r]|||^2 \cong \sum_K \eta_K^2([\boldsymbol{u}'', p'']), \tag{23}$$

where the symbol $\cong$ means to both terms in this expression have the same asymptotic behavior up to constants. Both sides of this approximation depend on time. For time dependent problems, the norm makes sense considering the maximum of the spatial estimates for all time steps or the discrete L^2 norm in time of these estimates.

In the next section we shall show that for the linearized stationary problem it is possible to prove that

$$|||[\boldsymbol{u} - \boldsymbol{u}_r, p - p_r]|||^2 \lesssim \sum_K \eta_K^2([\boldsymbol{u}'', p'']), \tag{24}$$

where $\lesssim$ stands for $\leq$ up to constants. In Section 5 we shall check the value of the effectivity index

$$\xi_{\text{eff}} := |||[\boldsymbol{u} - \boldsymbol{u}_r, p - p_r]||| \left(\sum_K \eta_K^2([\boldsymbol{u}'', p''])\right)^{-1/2},$$

in a numerical example in which $[\boldsymbol{u}, p]$ is known. Ideally, this number should be close to 1. However, it depends obviously on the values of the algorithmic constants c_1, c_2, c_3 appearing in Eqs. (8), (9) and (11). In fact, imposing that ξ_{eff} be as close to 1 as possible is a way to determine these algorithmic constants, i.e., they could be determined by minimizing $(\xi_{\text{eff}} - 1)^2$. Since the numerical unknowns depend on c_i, $i = 1, 2, 3$, this optimization problem would be hard to solve for the FE approximation, but not for the ROM. We comment further on this point in Section 5.

There is a major difference between the use of estimate (22) in the FE approximation and in the ROM. In the first case, that would naturally provide a criterion for adaptive mesh refinement: if η_K is above a certain threshold, the mesh should be refined, i.e., the local mesh size reduced according to the dependence of the a priori error estimate with h to have an error below the target. In the ROM case, however, the only possibility to act upon the error is to increase or decrease the ROM dimension, although this will have a global effect. A different situation is the use made in [42] of the a posteriori error estimate, where a FE mesh is used to compute the advection velocity of the ROM with an approximation coarser than the original FE mesh. The size of this coarser mesh can be determined by estimate (22).

4. Motivation results for the Oseen problem

In this section we prove (24) in the case of the linear stationary Oseen problem, in which the velocity $\boldsymbol{u}$ and the pressure p are solution of:

$$\begin{aligned}-\nu\Delta\boldsymbol{u} + \boldsymbol{a}\cdot\nabla\boldsymbol{u} + \nabla p &= \boldsymbol{f},\\ \nabla\cdot\boldsymbol{u} &= 0.\end{aligned}$$

For simplicity, we shall consider $\boldsymbol{u} = \boldsymbol{0}$ on $\partial\Omega$. The advection velocity $\boldsymbol{a}$ is given, and assumed to be solenoidal. The variational form of the problem consists of finding $\boldsymbol{u} \in V = H_0^1(\Omega)^d$ and $p \in Q$ such that

$$B_\Omega(\boldsymbol{a}; [\boldsymbol{u}, p], [\boldsymbol{v}, q]) = L_\Omega([\boldsymbol{v}, q]) \quad \forall [\boldsymbol{v}, q] \in V \times Q,$$

where B_Ω and L_Ω are given in Eqs. (1) and (2). The discrete problem consists in finding $[\boldsymbol{u}_r, p_r] \subset V_r \times Q_r$, such that

$$\begin{aligned}&B_\Omega(\boldsymbol{a}; [\boldsymbol{u}_r, p_r], [\boldsymbol{v}_r, q_r])\\ &\quad + \sum_K \langle \boldsymbol{u}_K'', \mathcal{L}_1^*(\boldsymbol{a}; [\boldsymbol{v}_r, q_r])\rangle_K - \sum_K \langle p_K'', \nabla\cdot\boldsymbol{v}_r\rangle_K\end{aligned}$$

$$- \sum_E \langle \boldsymbol{u}_E'', [\![\boldsymbol{n} \cdot \mathcal{F}^*(\boldsymbol{a}; [\boldsymbol{v}_r, q_r])]\!] \rangle_E$$
$$= L_\Omega([\boldsymbol{v}_r, q_r]) \quad \forall [\boldsymbol{v}_r, q_r] \in V_r \times Q_r, \tag{25}$$

$$\tau_{1,K}^{-1} \boldsymbol{u}_K'' = P^\perp(\boldsymbol{f} - \mathcal{L}_1(\boldsymbol{a}; [\boldsymbol{u}_r, p_r])), \tag{26}$$

$$\tau_{2,K}^{-1} p_K'' = -P^\perp(\nabla \cdot \boldsymbol{u}_r), \tag{27}$$

$$\tau_E^{-1} \boldsymbol{u}_E'' = -[\![\boldsymbol{n} \cdot \mathcal{F}([\boldsymbol{u}_r, p_r])]\!]. \tag{28}$$

Now the SGS given by Eqs. (26)–(28) can be inserted into Eq. (25), affecting also the right-hand-side, as $\boldsymbol{u}_K''$ depends on $\boldsymbol{f}$. Let us write the resulting problem as

$$B_S(\boldsymbol{a}; [\boldsymbol{u}_r, p_r], [\boldsymbol{v}_r, q_r]) = L_S([\boldsymbol{v}_r, q_r]), \tag{29}$$

for all $[\boldsymbol{v}_r, q_r] \in V_r \times Q_r$. The problem is consistent, i.e., the continuous solution $[\boldsymbol{u}, p]$ solves (29). Therefore, if we call $[\boldsymbol{e}_u, e_p] := [\boldsymbol{u} - \boldsymbol{u}_r, p - p_r]$, we have

$$B_S(\boldsymbol{a}; [\boldsymbol{e}_u, e_p], [\boldsymbol{v}_r, q_r]) = 0 \quad \forall [\boldsymbol{v}_r, q_r] \in V_r \times Q_r. \tag{30}$$

Let us take any $[\boldsymbol{v}, q] \in V \times Q$, fixed. Using Eq. (30) with $\boldsymbol{v}_r = P(\boldsymbol{v})$, $q_r = P(q)$, we have

$$\begin{aligned} &B_S(\boldsymbol{a}; [\boldsymbol{e}_u, e_p], [\boldsymbol{v}, q]) \\ &= B_S(\boldsymbol{a}; [\boldsymbol{e}_u, e_p], [P^\perp(\boldsymbol{v}), P^\perp(q)]) \\ &= L_S([P^\perp(\boldsymbol{v}), P^\perp(q)]) - \sum_K \langle \mathcal{L}(\boldsymbol{a}; [\boldsymbol{u}_r, p_r]), [P^\perp(\boldsymbol{v}), P^\perp(q)] \rangle_K \\ &\quad - \sum_K \langle \boldsymbol{n} \cdot \mathcal{F}([\boldsymbol{u}_r, p_r]), P^\perp(\boldsymbol{v}) \rangle_{\partial K} \\ &\quad - \sum_K \langle [\boldsymbol{u}_K'', p_K''], \mathcal{L}^*(\boldsymbol{a}; [P^\perp(\boldsymbol{v}), P^\perp(q)]) \rangle_K \\ &\quad - \sum_K \langle \boldsymbol{u}_E'', \boldsymbol{n} \cdot \mathcal{F}^*(\boldsymbol{a}; [P^\perp(\boldsymbol{v}), P^\perp(q)]) \rangle_{\partial K}, \end{aligned} \tag{31}$$

where we have made use of Eq. (4). Now we make the assumption that $\boldsymbol{f}$ is such that $L_S([P^\perp(\boldsymbol{v}), P^\perp(q)]) = 0$, which does not alter the accuracy of the formulation. Using standard interpolation estimates (see, e.g., [18]) and the expression of the stabilization parameters, it is found that

$$\sum_K \tau_{1,K}^{-1/2} \|P^\perp(\boldsymbol{v})\|_K \lesssim |||[\boldsymbol{v}, 0]|||, \tag{32}$$

$$\sum_K \tau_E^{-1/2} \|P^\perp(\boldsymbol{v})\|_{\partial K} \lesssim |||[\boldsymbol{v}, 0]|||, \tag{33}$$

$$\sum_K \tau_{2,K}^{-1/2} \|P^\perp(q)\|_K \lesssim |||[\boldsymbol{0}, q]|||, \tag{34}$$

$$\sum_K \tau_{1,K}^{1/2} \|P^\perp(\mathcal{L}_1(\boldsymbol{a}; [P^\perp(\boldsymbol{v}), P^\perp(q)]))\|_K \lesssim |||[\boldsymbol{v}, q]|||. \tag{35}$$

On the other hand, the stability of B_S, written in the form of inf-sup condition [13], implies that for $[\boldsymbol{e}_u, e_p] \in V \times Q$ there exists $[\boldsymbol{v}, q] \in V \times Q$ such that

$$|||[\boldsymbol{e}_u, e_p]||| \, |||[\boldsymbol{v}, q]||| \lesssim B_S(\boldsymbol{a}; [\boldsymbol{e}_u, e_p], [\boldsymbol{v}, q]).$$

Using this in Eq. (31) and bounds (32)–(35), we get

$$\begin{aligned} &|||[\boldsymbol{e}_u, e_p]||| \, |||[\boldsymbol{v}, q]||| \\ &\lesssim \sum_K \tau_{1,K}^{1/2} |||[\boldsymbol{v}, 0]||| \, \|P^\perp(\boldsymbol{f} - \mathcal{L}_1(\boldsymbol{a}; [\boldsymbol{u}_r, p_r]))\|_K \\ &\quad + \sum_K \tau_{2,K}^{1/2} |||[\boldsymbol{0}, q]||| \, \|P^\perp(\mathcal{L}_2(\boldsymbol{u}_r))\|_K \\ &\quad + \sum_E \tau_E^{1/2} |||[\boldsymbol{v}, 0]||| \, \|[\![\boldsymbol{n} \cdot \mathcal{F}([\boldsymbol{u}_r, p_r])]\!]\|_E \\ &\quad + \sum_K \tau_{1,K}^{-1/2} \|\boldsymbol{u}_K''\|_K \, |||[\boldsymbol{v}, q]||| + \sum_K \tau_{2,K}^{-1/2} \|p_K''\|_K \, |||[\boldsymbol{v}, q]||| \\ &\quad + \sum_E \tau_E^{-1/2} \|\boldsymbol{u}_E''\|_K \, |||[\boldsymbol{v}, q]|||, \end{aligned}$$

from where it follows that

$$|||[\boldsymbol{e}_u, e_p]||| \lesssim \sum_K \eta_K, \tag{36}$$

which is (24), the result we wanted to prove.

This result is only valid for the linearized and stationary problems, and it is only an upper bound. To establish the equivalence between $|||[\boldsymbol{e}_u, e_p]|||$ and $\Sigma_K \eta_K$ we should prove an estimate analogous to Eq. (36) with the inverse inequality $\gtrsim$ ($\geq$ up to constants). This is in general not possible, and the only way to check if approximation (23) is satisfied is through numerical experiments, one of which is presented in the next section.

Despite all its limitations, inequality (36) gives us confidence on the validity of the a posteriori error estimate we propose in the general transient and nonlinear problem. Moreover, from its deduction it is clearly seen why the stabilization parameters need to be used as scaling coefficients to have a dimensionally consistent estimate and (hopefully) equivalent to the norm in which the a priori numerical analysis is performed.

5. Numerical examples

5.1. An example with a manufactured solution

In this example we test the numerical behavior of the a posteriori error indicator proposed using a manufactured solution. We consider the square $\bar{\Omega} = [0, 1] \times [0, 1]$ and take the body forces so that the exact solution is

$$u_1(x_1, x_2, t) = f(x_1) f'(x_2) g(t),$$
$$u_2(x_1, x_2, t) = -f'(x_1) f(x_2) g(t),$$
$$p(x_1, x_2, t) = 10^5 x^2$$
$$f(x) = 100 x^2 (1 - x)^2,$$
$$g(t) = \cos(\pi t) \exp(-t),$$

where x_1 and x_2 are the Cartesian coordinates and u_1 and u_2 the velocity components. The viscosity is set to $\nu = 0.1$. To get a glimpse on the solution, the velocity field at $t = 2$ is plotted in Fig. 1.

We use this example to check the dependence of the statement in Eq. (23) on the algorithmic constants of the formulation we employ. We consider the domain discretized using a fine FE mesh

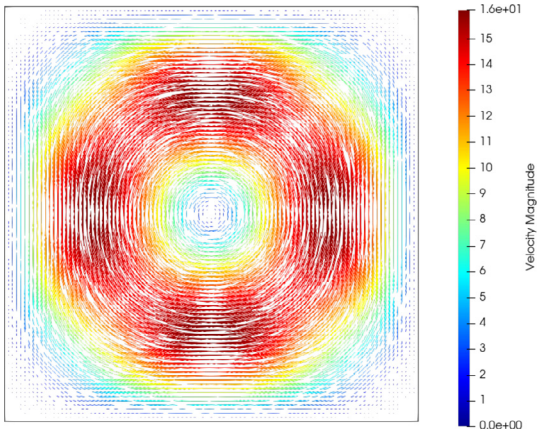

Fig. 1. Velocity vectors at $t = 2$.

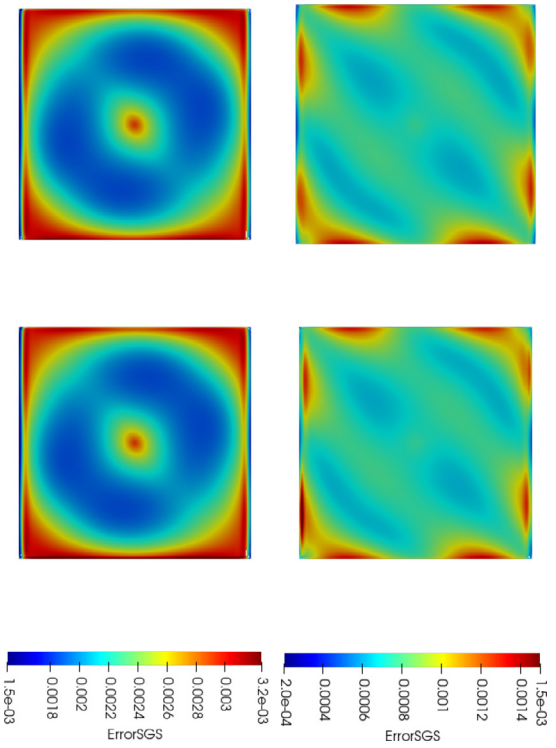

Fig. 2. Contours of the error indicator at $t = 2$. From the top to the bottom: FOM and ROM ($r = 5$). From the left to the right: constants $c_1 = 4$, $c_2 = 2$ (set I) and $c_1 = 16$, $c_2 = 4$ (set II).

of 100×100 bilinear elements to obtain the FOM solution, with a time step $\delta t = 0.0005$ and using a second order BDF2 scheme in time. To construct the ROM basis we use 1000 time snapshots gathered evenly every 10 time steps. We take $c_3 = 1$ in Eq. (11), and consider two sets of constants c_1 and c_2 in Eqs. (8) and (9), namely, those we use in all our applications, $c_1 = 4$, $c_2 = 2$, and $c_1 = 16$, $c_2 = 4$, which we have seen from trial and error that give a value of the effectivity index close to 1. We call the first set of constants set I and the second set II. Note that it can be justified that $c_1 \approx c_2^2$ [12].

In this very simple example, the ROM solution with $r = 5$ gives results already very close to the FOM, and thus this is the value of r we consider in all cases. The time step and time integrator scheme are the same as for the FOM.

Contours of the a posteriori error indicator in Eq. (22) are given in Fig. 2. It is observed there that the error predicted for the FOM is similar to that predicted for the ROM, whereas the set of constants I (the one we always employ in the applications) yields smaller predicted error than the set of constants II, in spite of the fact that the latter yields an effectivity index close to 1.

The time evolution of the exact global error is plotted in Fig. 3. As mentioned earlier, the FOM and the ROM have similar errors, particularly for the set of constants I, for which the error is smaller than for the set II.

The time evolution of the a posteriori global error indicator is plotted in Fig. 4. Here the error predicted using the set of constants II is smaller than for the set I, and the FOM and ROM solutions have virtually the same error.

As a result of Figs. 3 and 4, the evolution of the effectivity index is shown in Fig. 5. The set of constants II has an index close to 1, although the error is higher that for the set of constants I.

As a conclusion, we observe that although Eq. (23) may hold (and one of the inequalities has been proven for a simplified problem in Section 4), the constants involved in this expression depend

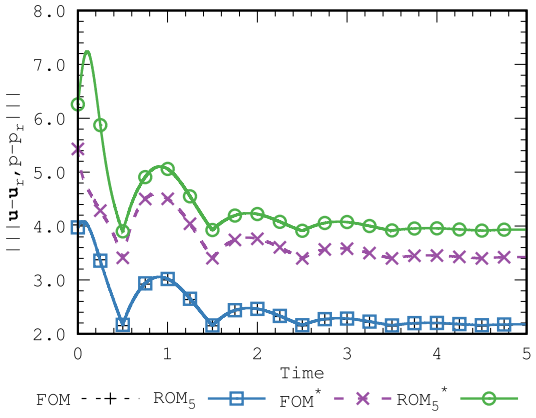

Fig. 3. Time evolution of the exact error for the FOM and the ROM ($r = 5$) with constants $c_1 = 4$, $c_2 = 2$ (set I) and $c_1 = 16$, $c_2 = 4$ (set II), the latter indicated with an asterisk.

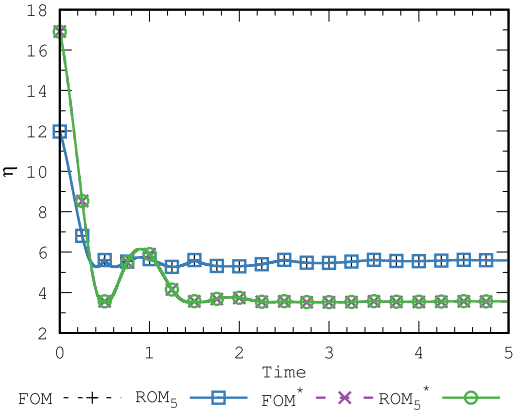

Fig. 4. Time evolution of the a posteriori error indicator for the FOM and the ROM ($r = 5$) with constants $c_1 = 4$, $c_2 = 2$ (set I) and $c_1 = 16$, $c_2 = 4$ (set II), the latter indicated with an asterisk.

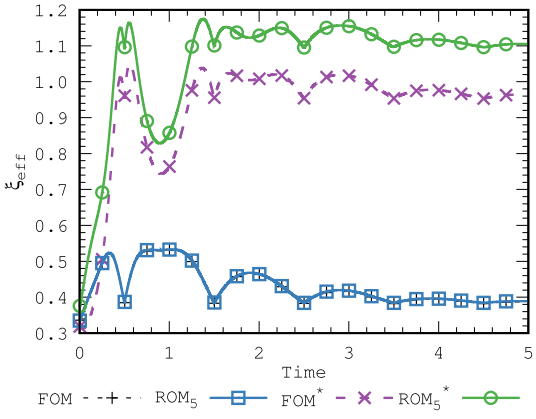

Fig. 5. Time evolution of the effectivity index for the FOM and the ROM ($r = 5$) with constants $c_1 = 4$, $c_2 = 2$ (set I) and $c_1 = 16$, $c_2 = 4$ (set II), the latter indicated with an asterisk.

on different factors, and in particular on the algorithmic constants of the formulation. Adjusting them to have an effectivity index close to 1 does not mean that the true error is better that when this index is far from unity.

5.2. Flow over a backward facing step

This numerical example consist in a two dimensional flow over a backward facing step similar to the one presented in [31] and

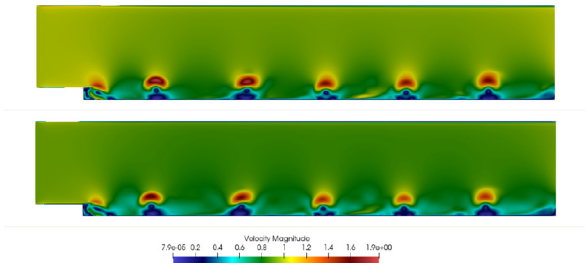

Fig. 6. Velocity norm at $t = 50$. Top: FOM, bottom: ROM ($r = 10$).

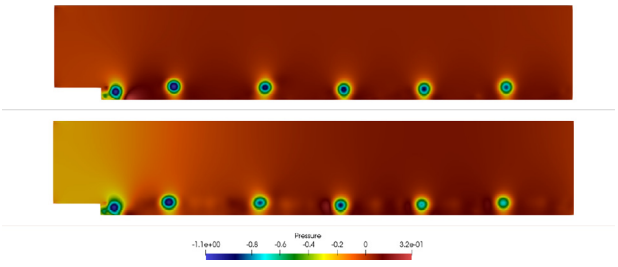

Fig. 7. Pressure contours at $t = 50$. Top: FOM, bottom: ROM ($r = 10$).

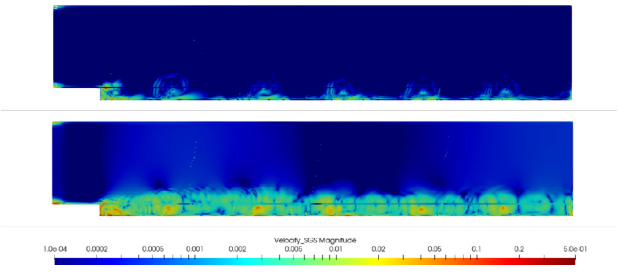

Fig. 8. Norm of the velocity SGS at $t = 50$. Top: FOM, bottom: ROM ($r = 10$).

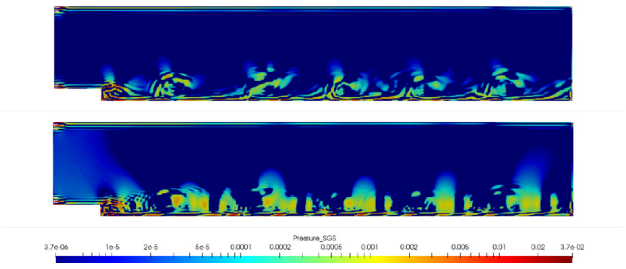

Fig. 9. Contours of pressure SGS at $t = 50$. Top: FOM, bottom: ROM ($r = 10$).

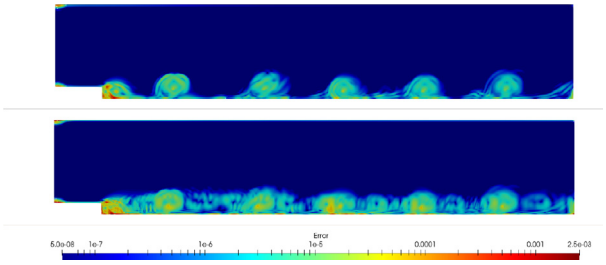

Fig. 10. Element-wise a posteriori error indicator η at $t = 50$. Top: FOM, bottom: ROM ($r = 10$).

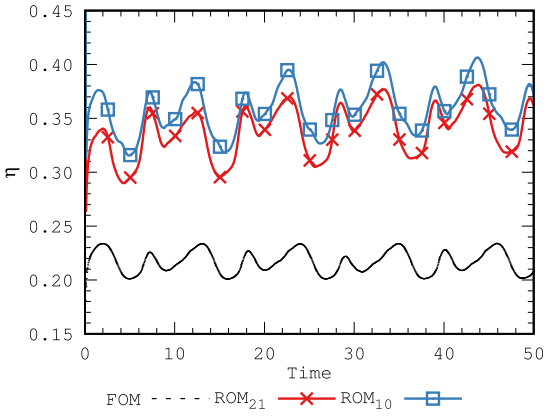

Fig. 11. Time evolution of the global a posteriori error indicator η for the FOM, the ROM with $r = 10$ and the ROM with $r = 21$.

solved using model reduction in [4,5]. The computational domain is the rectangle $[0, 44] \times [0, 9]$, with a unit length step placed at (4,0). The inflow velocity at $x = 0$ is prescribed to (1.0,0), whereas at the lower and upper boundaries a wall law boundary condition is set with the wall distance characterizing the wall model $\delta = 0.001$. The outflow (where both the x and y velocity components are left free) is set at $x = 44$. The viscosity is prescribed to $\nu = 0.00005$, resulting in a Reynolds number of 20000. The domain is discretised using a symmetric mesh of 61520 quadrilateral bilinear elements and 62214 nodes for the FOM.

We perform a preliminary simulation until $t = 100$ and use the velocity and pressure solutions of the next 1000 time steps as snapshots to calculate the basis. A time step of $\delta t = 0.05$ is used in both the FOM and the ROM cases.

Figs. 6 and 7 show contours of velocity norm and pressure at $t = 50$, respectively, for both the FOM and the ROM using a dimension of the ROM space $r = 10$. They are only intended to show the flow pattern and how the ROM is able to approximate the FOM solution.

Figs. 8 and 9 show contours of the norm of the velocity SGS and the pressure SGS at $t = 50$, respectively, for both the FOM and the ROM using a dimension of the ROM space $r = 10$. These figures serve to show that the SGS are more relevant for the ROM than for the FOM, as expected.

From the velocity and pressure SGS we may construct our a posteriori error indicator, given for each element and for each time step in Eq. (22). In this numerical example, this quantity is represented in Fig. 10 at $t = 50$ for both the FOM and the ROM. As expected, this indicator predicts higher error in the ROM than in the FOM.

The time evolution of the global a posteriori error indicator η, obtained from the sum of the contributions of all the elements, is represented in Fig. 11 for the FOM, the ROM with $r = 10$ and the ROM with $r = 21$. The time average of η for different values of r is shown in Fig. 12. It is observed that roughly the error is 0.22 for the FOM and 0.38 for the ROM with $r = 8$, decreasing up to 0.34 when $r = 21$. It is difficult to decrease the ROM error further because of the over-fitting effect usually encountered in ROM.

In this numerical example we do not have any reference solution that could be considered 'exact' and taken as a reference. Yet, we may try to plot a crude approximation to the effectivity index (ξ^*_{eff}) for the ROM assuming the FOM to be the reference solution and the a posteriori error estimate for the FOM to be the true error. This of course will produce a very rough estimate of the effectivity index since, according to Fig. 12, the error for the ROM with $r = 21$ is only 55% higher than for the FOM. The result of this is represented in Fig. 13. The important message of this figure is that the approximation considered to the effectivity index grows with r, and in this case tends to roughly 0.64.

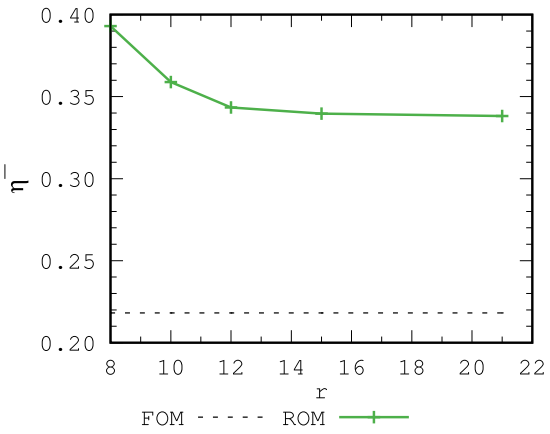

Fig. 12. Time average of the global a posteriori error indicator η for the FOM and the ROM with different values of r.

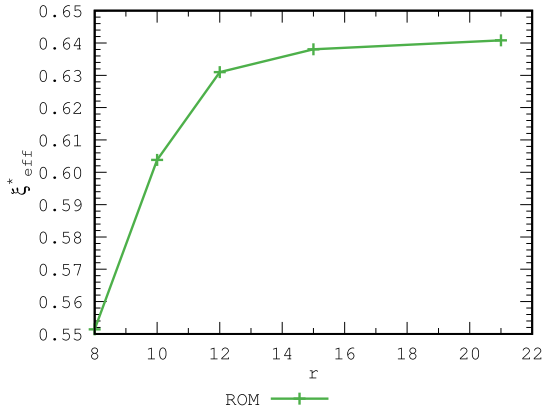

Fig. 13. Approximated effectivity index for different values of r taking the FOM as a reference solution.

6. Conclusion

In this paper we have presented an a posteriori error estimate for the ROM approximation of the incompressible Navier-Stokes equations, assuming that the FOM is a VMS-type FE method. This estimate can also be used for the FOM, the usage being more limited in the ROM. While in the FOM it naturally leads to an adaptive mesh refinement algorithm, in the ROM, in principle, only determines the need or not to increase the ROM dimension. However, some ideas in the direction of introducing adaptivity for the ROM have been discussed in this paper.

The a posteriori error estimate presented has to be understood in the norm in which the a priori analysis can be performed, i.e., it is not any standard norm of functions, but a combination of norms of different terms scaled by mesh dependent parameters. It has been explained why these parameters are the same in the ROM and in the FOM. It is also remarkable that this norm introduces the adequate combination of error in velocity and pressure.

Confidence on the a posteriori error estimate presented comes from two sources. First, we have shown analytically that it provides an upper bound for the true error in the case of the stationary and linearized problem. Second, the numerical examples show that it has the correct numerical behavior. Moreover, in the case of the example with a manufactured solution we have explained how the algorithmic constants of the formulation can be adjusted so as to obtain an effectivity index close to one.

Declaration of Competing Interest

On behave of the rest of authors, I declare that we do not have any conflict of interest.

Acknowledgments

R. Codina acknowledges the support received from the ICREA Acadèmia Research Program, from the Catalan Government. R. Reyes acknowledges the scholarship received from COLCIENCIAS, from the Colombian Government. J. Baiges acknowledges the support of the Spanish Government through the Ramón y Cajal grant RYC-2015-17367. This work was partially funded through the TOP-FSI: RTI2018-098276-B-I00 project of the Spanish Government.

References

[1] D. Amsallem, C. Farhat, Stabilization of projection-based reduced-order models, Int. J. Numer. Methods Eng. 91 (4) (2012) 358–377, doi:10.1002/nme.4274.
[2] M. Azaïez, T. Chacón-Rebollo, S. Rubino, Streamline derivative projection-based POD-ROM for convection-dominated flows. part i: numerical analysis, arXiv preprint (2017).
[3] J. Baiges, R. Codina, Variational multiscale error estimators for solid mechanics adaptive simulations: an orthogonal subgrid scale approach, Comput. Methods Appl. Mech. Eng. 325 (2017) 37–55, doi:10.1016/j.cma.2017.07.008.
[4] J. Baiges, R. Codina, S. Idelsohn, Explicit reduced-order models for the stabilized finite element approximation of the incompressible Navier-Stokes equations, Int. J. Numer. Methods Fluids 72 (12) (2013) 1219–1243, doi:10.1002/fld.3777.
[5] J. Baiges, R. Codina, S. Idelsohn, Reduced-order subscales for POD models, Comput. Methods Appl. Mech. Eng. 291 (2015) 173–196.
[6] M. Balajewicz, E.H. Dowell, Stabilization of projection-based reduced order models of the navier-Stokes, Nonlinear Dyn. 70 (2) (2012) 1619–1632, doi:10.1007/s11071-012-0561-5.
[7] M. Barrault, Y. Maday, N.C. Nguyen, A.T. Patera, An empirical interpolation method: application to efficient reduced-basis discretization of partial differential equations, C.R. Math. 339 (9) (2004) 667–672, doi:10.1016/j.crma.2004.08.006.
[8] M. Bergmann, C.H. Bruneau, A. Iollo, Enablers for robust POD models, J. Comput. Phys. 228 (2) (2009) 516–538, doi:10.1016/j.jcp.2008.09.024.
[9] E. Burman, M.A. Fernández, P. Hansbo, Continuous interior penalty finite element method for Oseen's equations, SIAM J. Numer. Anal. 44 (3) (2006) 1248–1274, doi:10.1137/040617686.
[10] K. Carlberg, Adaptive h -refinement for reduced-order models, Int. J. Numer. Methods Eng. 102 (5) (2015) 1192–1210, doi:10.1002/nme.4800.
[11] K. Carlberg, C. Bou-Mosleh, C. Farhat, Efficient non-linear model reduction via a least-squares Petrov-Galerkin projection and compressive tensor approximations, Int. J. Numer. Methods Eng. 86 (2) (2011) 155–181, doi:10.1002/nme.3050.
[12] R. Codina, Stabilized finite element approximation of transient incompressible flows using orthogonal subscales, Comput. Methods Appl. Mech. Eng. 191 (2002) 4295–4321.
[13] R. Codina, Analysis of a stabilized finite element approximation of the Oseen equations using orthogonal subscales, Appl. Numer. Math. 58 (2008) 264–283.
[14] R. Codina, S. Badia, J. Baiges, J. Principe, Variational Multiscale Methods in Computational Fluid Dynamics, in Encyclopedia of Computational Mechanics E. Stein, T.J.R. Hughes, John Wiley & Sons Ltd., pp. 1–28. 10.1002/9781119176817.ecm2117
[15] R. Codina, J. Principe, J. Baiges, Subscales on the element boundaries in the variational two-scale finite element method, Comput. Methods Appl. Mech. Eng. 198 (2009) 838–852.
[16] J.L. Eftang, A.T. Patera, E.M. Rønquist, An "hp" certified reduced basis method for parametrized elliptic partial differential equations, SIAM J. Scient. Comput. 32 (6) (2010) 3170–3200, doi:10.1137/090780122.
[17] L. El Alaoui, A. Ern, Residual and hierarchical a posteriori error estimates for nonconforming mixed finite element methods, ESAIM Math. Model. Numer. Anal. 38 (6) (2004) 903–929, doi:10.1051/m2an:2004044.
[18] A. Ern, J.-L. Guermond, Theory and Practice of Finite Elements, Springer-Verlag, 2004.
[19] P.A. Etter, K.T. Carlberg, Online adaptive basis refinement and compression for reduced-order models via vector-space sieving, arXiv e-print (2019).
[20] M. Fahl, Computation of POD basis functions for fluid flows with Lanczos methods, Math. Comput. Model 7177 (01) (2001).
[21] S. Giere, Numerical and Analytical Aspects of POD-Based Reduced-Order Modeling in Computational Fluid Dynamics, Freien Universität Berlin, 2016 Ph.D. thesis.
[22] S. Giere, T. Iliescu, V. John, D. Wells, SUPG Reduced order models for convection-dominated convection-diffusion-reaction equations, Comput. Methods Appl. Mech. Eng. 289 (2015) 454–474, doi:10.1016/j.cma.2015.01.020.
[23] B. Haasdonk, M. Dihlmann, M. Ohlberger, A training set and multiple bases generation approach for parameterized model reduction based on adaptive

grids in parameter space, Math. Comput. Model Dyn. Syst. 17 (4) (2011) 423–442, doi:10.1080/13873954.2011.547674.
[24] J.S. Hale, E. Schenone, D. Baroli, L. Beex, S. Bordas, A hyper-reduction method using adaptivity to cut the assembly costs of reduced order models, e-print (2019).
[25] G. Hauke, M.H. Doweidar, M. Miana, The multiscale approach to error estimation and adaptivity, Comput. Methods Appl. Mech. Eng. 195 (13–16) (2006) 1573–1593, doi:10.1016/j.cma.2005.05.029.
[26] G. Hauke, D. Fuster, F. Lizarraga, Variational multiscale a posteriori error estimation for systems: The Euler and Navier-Stokes equations, Comput. Methods Appl. Mech. Eng. 283 (2015) 1493–1524, doi:10.1016/j.cma.2014.10.032.
[27] J. Hernández, M. Caicedo, A. Ferrer, Dimensional hyper-reduction of nonlinear finite element models via empirical cubature, Comput. Methods Appl. Mech. Eng. 313 (2017) 687–722, doi:10.1016/j.cma.2016.10.022.
[28] T. Hughes, G. Feijóo, L. Mazzei, J. Quincy, The variational multiscale method–a paradigm for computational mechanics, Comput. Methods Appl. Mech. Eng. 166 (1998) 3–24.
[29] T. Iliescu, Z. Wang, Variational multiscale proper orthogonal decomposition: convection-dominated convection-diffusion-reaction equations, Math. Comput. 82 (283) (2013) 1357–1378, doi:10.1090/S0025-5718-2013-02683-X.
[30] T. Iliescu, Z. Wang, Variational multiscale proper orthogonal decomposition: Navier-Stokes equations, Numer. Methods Partial. Differ. Equ. 30 (2) (2014) 641–663, doi:10.1002/num.21835.
[31] S. Jovic, An Experimental Study of a Separated/Reattached Flow Behind a Backward-Facing Step. Re=37000, Technical Report, National Aeronautics and Space Administration, Ames Research Center, 1996.
[32] I. Kalashnikova, M.F. Barone, S. Arunajatesan, B.G. Van Bloemen Waanders, Construction of energy-stable projection-based reduced order models, Appl. Math. Comput. 249 (2014) 569–596, doi:10.1016/j.amc.2014.10.073.
[33] B. Kragel, Streamline Diffusion POD Models in Optimization, University of Trier, 2005 Ph.D. thesis.
[34] M.G. Larson, A. Målqvist, Adaptive variational multiscale methods based on a posteriori error estimation: energy norm estimates for elliptic problems, Comput. Methods Appl. Mech. Eng. 196 (21) (2007) 2313–2324.
[35] M.G. Larson, A. Målqvist, An adaptive variational multiscale method for convection–diffusion problems, Commun. Numer. Methods Eng. 25 (1) (2009) 65–79.
[36] I. Martini, G. Rozza, B. Haasdonk, Reduced basis approximation and a-posteriori error estimation for the coupled stokes-darcy system, Adv. Comput. Math. 41 (2015) 1131–1157.
[37] A. Masud, T.J. Truster, L.A. Bergman, A variational multiscale a posteriori error estimation method for mixed form of nearly incompressible elasticity, Comput. Methods Appl. Mech. Eng. 200 (47) (2011) 3453–3481.
[38] B. McLaughlin, J. Peterson, M. Ye, Stabilized reduced order models for the advection-diffusion-reaction equation using operator splitting, Comput. Math. Appl. 71 (11) (2016) 2407–2420, doi:10.1016/j.camwa.2016.01.032.
[39] N.C. Nguyen, A.T. Patera, J. Peraire, A best point interpolation method for efficient approximation of parametrized functions, Int. J. Numer. Methods Eng. 73 (4) (2008) 521–543, doi:10.1002/nme.2086.
[40] B. Peherstorfer, K. Willcox, Online adaptive model reduction for nonlinear systems via low-Rank updates, SIAM J. Scient. Comput. 37 (4) (2015) A2123–A2150, doi:10.1137/140989169.
[41] B. Peherstorfer, K. Willcox, Dynamic data-driven model reduction: adapting reduced models from incomplete data, Adv. Model. Simul. Eng. Sci. 3 (1) (2016) 11, doi:10.1186/s40323-016-0064-x.
[42] R. Reyes, R. Codina, Element boundary terms in reduced order models for flow problems: Domain decomposition and adaptive coarse mesh hyper-reduction, Comput. Methods Appl. Mech. Eng. 368 (2020) 113159, doi:10.1016/j.cma.2020.113159.
[43] R. Reyes, R. Codina, Projection-based reduced order models for flow problems: a variational multiscale approach, Comput. Methods Appl. Mech. Eng. 363 (2020) 112844, doi:10.1016/j.cma.2020.112844.
[44] S. Rubino, A streamline derivative POD-ROM for advection-diffusion-reaction equations, ESAIM: Proc. Surveys 64 (June) (2018) 121–136, doi:10.1051/proc/201864121.
[45] D. Ryckelynck, F. Vincent, S. Cantournet, Multidimensional a priori hyper-reduction of mechanical models involving internal variables, Comput. Methods Appl. Mech. Eng. 225–228 (2012) 28–43, doi:10.1016/j.cma.2012.03.005.
[46] G. Stabile, F. Ballarin, G. Zuccarino, G. Rozza, A reduced order variational multiscale approach for turbulent flows, Adv. Comput. Math. 45 (2019) 2349–2368.
[47] A. Thari, V. Pasquariello, N. Aage, S. Hickel, Adaptive reduced-Order modeling for non-Linear fluid-Structure interaction, arxiv e-print (2017).
[48] S. Ullmann, M. Rotkvic, J. Lang, POD-Galerkin Reduced-order modeling with adaptive finite element snapshots, J. Comput. Phys. 325 (2016) 244–258, doi:10.1016/j.jcp.2016.08.018.
[49] S. Volkwein, Proper orthogonal decomposition: theory and reduced-Order modelling, 2013.
[50] Z. Wang, I. Akhtar, J. Borggaard, T. Iliescu, Two-level discretizations of nonlinear closure models for proper orthogonal decomposition, J. Comput. Phys. 230 (1) (2011) 126–146, doi:10.1016/j.jcp.2010.09.015.
[51] D. Wells, Z. Wang, X. Xie, T. Iliescu, An evolve-then-filter regularized reduced order model for convection-dominated flows, Int. J. Numer. Methods Fluids 84 (10) (2017) 598–615, doi:10.1002/fld.4363.